PERGAMON

International Journal of Heat and Mass Transfer 43 (2000) 3687–3700

International Journal of HEAT and MASS TRANSFER

www.elsevier.com/locate/ijhmt

Experimental and numerical characterisation of mixing in a steady spatially chaotic flow by means of residence time distribution measurements

C. Castelain[a,*], D. Berger[a], P. Legentilhomme[b], A. Mokrani[a], H. Peerhossaini[a]

[a]*Thermofluids and Complex Flows Research Group, Laboratoire de Thermocinétique, UMR CNRS 6607, ISITEM, Université de Nantes, La Chantrerie, CP 3023, F 44087 Nantes Cedex 03, France*

[b]*Laboratoire de Génie des Procédés, Institut Universitaire de Technologie, Département Génie Chimique, BP 420, F 44606 Saint-Nazaire Cedex, France*

Received 6 November 1998; received in revised form 27 September 1999

Abstract

This work describes an experimental study and a numerical simulation of residence time distributions (RTD) in a spatially chaotic three-dimensional flow. The experimental system is made up of a succession of bends in which centrifugal force generates a pair of streamwise Dean roll-cells. Fluid particle trajectories become chaotic through geometrical perturbation obtained by rotating the curvature plane of each bend $\pm 90^\circ$ with respect to the neighbouring ones. Different numbers of bends, ranging from 3 to 33, were tested. RTD is experimentally obtained by using a two-measurement-point conductimetric method, the concentration of the injected tracer being determined both at the inlet and at the outlet of the chaotic mixer. The experimental RTD is modelled by a plug flow with axial dispersion volume exchanging mass with a stagnant zone. RTD experiments were conducted for Reynolds numbers between 30 and 13,000. Péclet number based on the diameter of the pipe $Pe_D = \frac{\bar{W}D}{D_{ax}}$) increases with Reynolds number, whatever the number of bends in the system. This reduction in axial dispersion is due to the secondary Dean flow and the chaotic trajectories. Globally, the flowing fraction increases with Reynolds number, whatever the number of bends, to reach a maximum value between 90 and 100%. For Reynolds numbers between 50 and 200, the flowing fraction increases with the number of bends. The stagnant zone models fluid particles located close to the tube wall. The pathlines become progressively chaotic in small zones in the cross section and then spread across the flow as the number of bends is increased, allowing more trapped particles to move towards the tube centre. In order to characterise more completely the efficiency of the device, a criterion is proposed that takes into account both the mixing characteristics and the pressure drop. The RTD for low Reynolds numbers has also been obtained numerically using a flow model based on Dean's asymptotic perturbation solutions of the mean flow in a curved pipe. At the end of each bend, the velocity field is rotated by $\pm 90^\circ$ before entering the next bend. The RTD is calculated by following the trajectories of 250,000 'numerical' particles along the device. Numerical results are in good agreement with experiments in the same Reynolds number range.

* Corresponding author. Tel.: +33-2-40-68-31-47; fax: 33-2-40-68-31-41.

E-mail address: cast@isitem.univ-nantes.fr (C. Castelain).

0017-9310/00/$ - see front matter
PII: S0017-9310(99)00363-4

Nomenclature

A	Dimensionless number, $A = -\frac{R^2}{\mu \bar{W}} \frac{\partial P}{R_c \partial \theta}$
C	Concentration of an injected tracer (mol m^{-3})
C^*	Concentration of an injected tracer in the stagnant zone (mol m^{-3})
$C_1(t)$	Concentration of an injected tracer at the inlet (mol m^{-3})
$C_2(t)$	Concentration of an injected tracer at the outlet (mol m^{-3})
$C_1'(t)$	Normalised concentration of an injected tracer at the inlet
$C_2'(t)$	Normalised concentration of an injected tracer at the outlet
C_f	Friction factor
C_r	Mixing criterion, $C_r = \frac{\nu}{D_{ax} C_f}$
D	Tube diameter (m)
D_{ax}	Axial dispersion coefficient (m^2 s^{-1})
Dn	Dean number, $Dn = Re\sqrt{\frac{D}{R_c}}$
RMS	Root mean square error (%)
f	Fraction of volume subjected to flow
$F(s)$, $F_1(s)$, $F_2(s)$, $F_3(s)$	Transfer functions
G	Dimensionless group, $G = \frac{KL}{\bar{W}}$
K	Mass transfer coefficient between the flowing volume and the stagnant region (s^{-1})
L	Total length of the system (m)
P	Pressure (Pa)
Pe_D	Péclet number based on the diameter of the system, $Pe_D = \frac{\bar{W}D}{D_{ax}}$
Pe_L	Péclet number based on the total length of the system, $Pe_L = \frac{\bar{W}L}{D_{ax}}$
r	Local radial coordinate (m)
R	Tube radius (m)
R_c	Mean curvature radius (m)
Re	Reynolds number, $Re = \frac{\bar{W}D}{\nu}$
t	Time (s)
$\overline{t_s}$	Mean residence time (s)
u, v	Secondary velocity components (m s^{-1})
w	Axial velocity (m s^{-1})
$\bar{W}$	Average axial velocity (m s^{-1})
x, y, θ and r, φ, θ	Toroidal local coordinate systems
z	Streamwise coordinate (m)
Greek symbols	
α	Angle between two successive bends (°)
β	Dimensionless number, $\beta = Pe_L^2 + 4s\gamma Pe_L \overline{t_s}$
θ, φ	Local angular coordinates (rad)
γ	Dimensionless number, $\gamma = f + \frac{G(1-f)}{\overline{t_s} s(1-f)+G}$
μ	Dynamic viscosity (Pa s)
ν	Kinematic viscosity, (m^2 s^{-1})
ρ	Fluid density (kg m^{-3})
ψ	Stream function
ω	Pulsation of the Fourier series (rad s^{-1})

1. Introduction

Techniques commonly used to enhance mixing often involve the generation of turbulent flow. In some cases, however, fluids with long molecular chains can be damaged by high shear stresses, and also energy is lost by turbulent agitation. In the regular laminar regime, mixing is induced mainly by molecular diffusion. The idea of generating a spatial (Lagrangian) chaotic behaviour from a deterministic flow by simple geometrical perturbations has attracted much attention in recent years [1–3], in large part because of its potential application in mixing devices [4–7].

The geometrical perturbation induces complex three-dimensional chaotic trajectories in which particles can visit a large number of positions in physical space. To generate chaotic flow paths, we used the same technique as Peerhossaini et al. [8], which exploits the secondary flow patterns, usually known as Dean roll-cells [3]. The secondary flow is a pair of counter-rotating vortices projected in the duct cross-section [9,10]. In a curved pipe, the secondary flow pattern is closely linked to the channel curvature. By shifting the plane of curvature from one bend to the next, one can induce a class of trajectories in one bend, then deform it to another type in the next bend, and so on. Very

complex flow paths can be produced in this way, and a fluid particle undergoing such flows follows a chaotic path. Such chaotic cross-sectional movement has been found to enhance the advection of passive scalars and therefore to improve the efficiency of the wall heat transfer, leading to homogenisation in the fluid volume [8,11] and thus better mixing.

A commonly used diagnostic for continuous mixing is the residence time distribution (RTD), which lets one obtain a global dispersion coefficient by using an appropriate model. In previous work [7], we compared RTD in helically coiled and chaotic twisted pipe for Reynolds numbers between 800 and 13,000 and for different numbers of bends. In order to investigate dispersion in the two experimental arrangements, we used the axial dispersion plug flow model. For Reynolds numbers larger than 2500, axial dispersion in the chaotic system is more than 20% less than in a helically coiled tube having the same number of bends. The decrease in axial dispersion is due to the generation of chaotic trajectories, which also contribute to an increase in transverse dispersion. For smaller

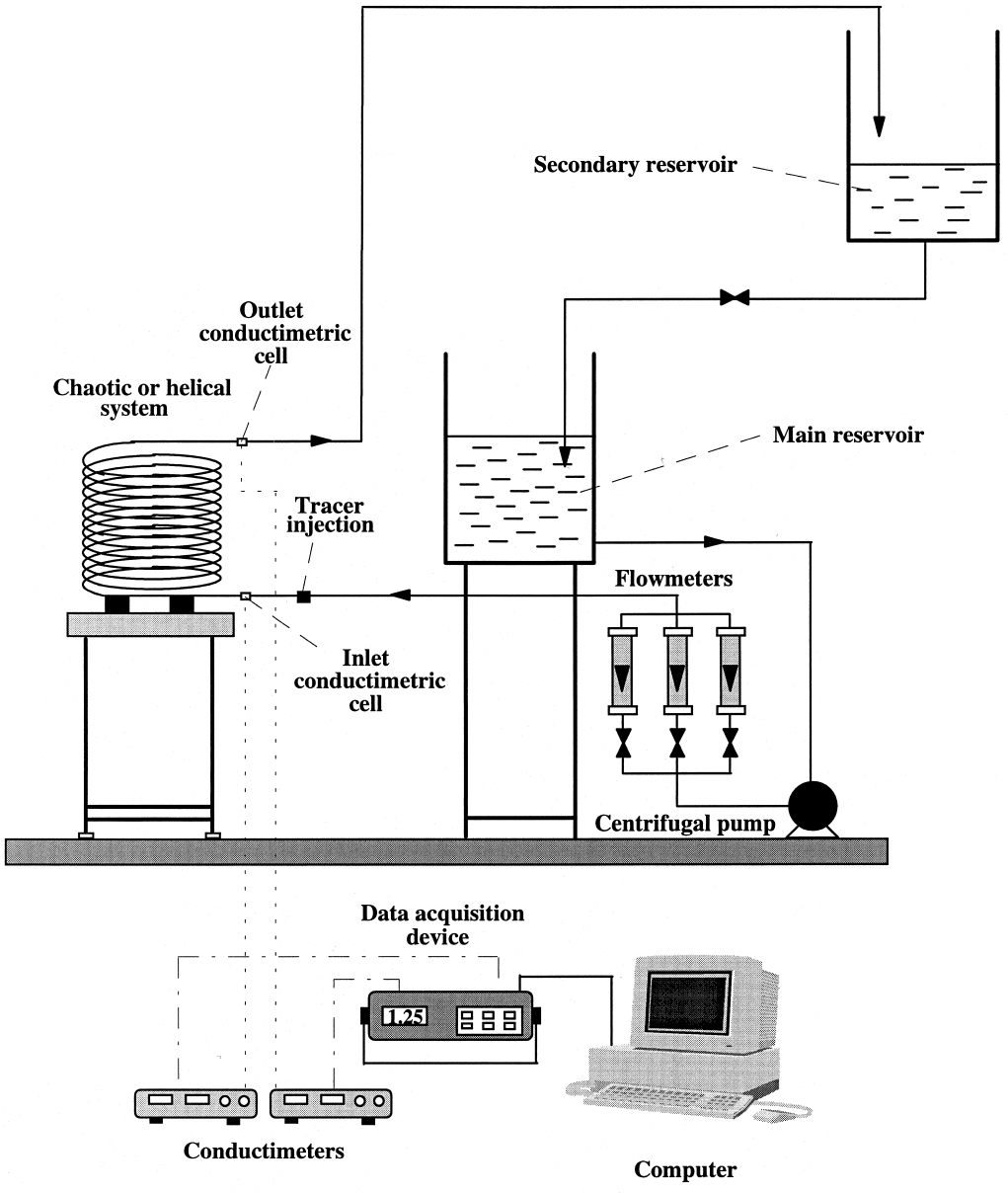

Fig. 1. Schematic diagram of the flow loop.

Reynolds numbers, the agreement between the plug flow with axial dispersion model and the experimental RTD curves was not satisfactory, a disagreement primarily attributed to the long tails of the experimental RTDs.

In the previous work [7], water was used as the working fluid for Reynolds numbers between 800 and 13,000. In the present study, we use two saccharose solutions so that the Reynolds number varies between 30 and 1700. The objective of this study is to characterise experimentally the mixing properties in the chaotic system for this range of Reynolds numbers. For smaller Reynolds numbers ($Re < 100$), a numerical simulation of the RTD is also presented in both a helically coiled and a chaotic system. The mixing characteristics in both configurations will be compared, as well as numerical results and experimental data.

The experimental apparatus and methods are described in the next section. The third section covers the modelling of the experimental RTD and analysis of the experimental data, while the fourth section deals with the results of the numerical simulation of RTD in the same geometry. Numerical and experimental data are compared in the final part of the paper.

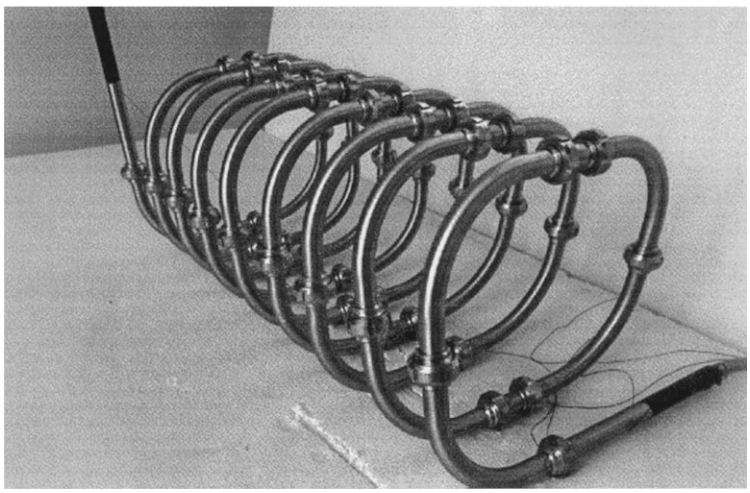

(a)

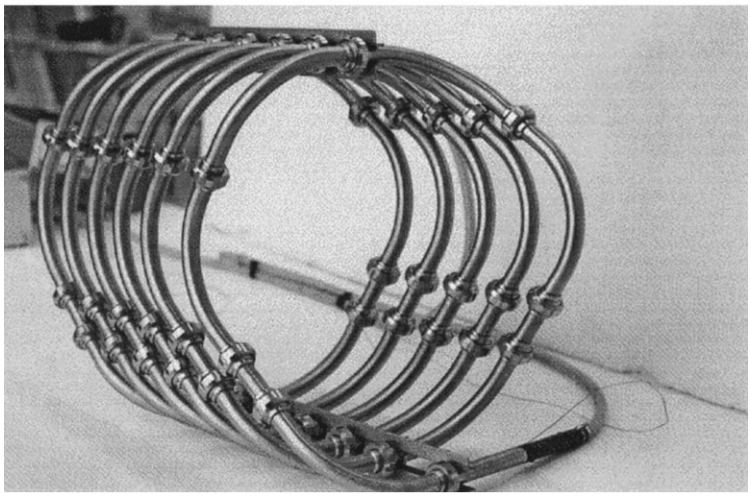

(b)

Fig. 2. The two systems under study: (a) helically coiled tube; (b) chaotic configuration.

2. Experimental apparatus and methods

2.1. Flow loop and working fluid

The experimental flow loop, previously described by Castelain et al. [7], is schematically depicted in Fig. 1. The setup consists of an overhead reservoir of volume about 0.2 m^3, from which the working liquid is circulated by means of a centrifugal pump. The flow rate is measured by three calibrated flowmeters, connected in parallel, in the range 0.03–0.84 $m^3\ h^{-1}$ with an accuracy of $\pm 1.5\%$ over the whole flow rate range. Before entering the test section, i.e. the chaotic or helically coiled system (see Fig. 1), the liquid flows through a straight pipe 3 m long, more than 65 times the inner diameter of the curved tubes. The presence of this pipe ensures an axial fully developed flow field at the inlet of the test section in the range of Reynolds numbers under study (30–13,000).

In the present study, as well as in the previous work [7], the helical and chaotic mixers are both made of 33 identical bends. Each bend consists of a 90° curved stainless-steel tube of circular cross-section, the inner and outer radii of which are 23 and 25 mm, respectively. The mean radius of curvature of the bends is 126.5 mm, which yields a mean curvature ratio of 0.18. The bends can be assembled so as either to form a helically coiled pipe or to generate chaotic fluid particle paths. The complete helical system consists of 33 bends, connected by 16 straight sections of 55-mm lengths (Fig. 2(a)). The chaotic twisted pipe device is also made of 33 bends and 11 straight sections of 80-mm length (Fig. 2(b)). The latter geometry is obtained by shifting the plane of curvature of each bend by a 90° angle with respect to the previous one. Both complete helically coiled and chaotic twisted pipe systems have the same overall length, about 10 m. Different configurations, made up of 3 to 33 bends, were tested in order to investigate their effect on the mixing properties in both geometries (see Table 1). In our previous work [7], water was used as the working fluid for Reynolds numbers ranging between 800 and 13,000. In the present study, we used two saccharose solutions, allowing a Reynolds number variation between 30 and 1700. The geometrical characteristics of the configurations studied and the hydrodynamical parameters are summarised in Table 1. During the RTD experiments, the working fluid is not recycled so as to avoid any modification of its physical properties, but is instead stored in a second reservoir, as shown in Fig. 1. The pressure drops induced by both the twisted pipe device and helically coiled tube were measured using small pressure tabs mounted flush to the pipe wall at the inlet and outlet of the system and connected to an inclined U-differential manometer.

Table 1
Geometrical and hydrodynamical parameters of the studied configurations

	Lengths of the studied configurations			
	Number of bends	Curved length (m)	Straight length (m)	Total length (m)
Hellically coiled system	3	0.596	0.295	0.891
	9	1.788	0.935	2.723
	15	2.981	1.585	4.566
	21	4.173	2.230	6.403
	27	5.365	2.875	8.240
	33	6.557	3.521	10.078
Chaotic system	3	0.596	0.320	0.916
	6	1.192	0.640	1.832
	9	1.788	0.960	2.748
	15	2.981	1.600	4.581
	21	4.173	2.240	6.413
	27	5.365	2.880	8.245
	33	6.557	3.520	10.078
	Experimental domain			
	System	Number of bends	Viscosity of the liquid (Pa s)	*Re* range
Castelain et al. [7]	Helically coiled	3, 9, 15, 21, 27, 33	10^{-3} (water)	800–13,000
	Chaotic	3, 9, 15, 21, 27, 33	10^{-3} (water)	800–13,000
Present work	Chaotic	3, 6, 9, 33	0.102–0.128 (saccharose)	30–200
	Chaotic	3, 6, 33	0.012 (saccharose)	400–1700

2.2. Experimental determination of the residence time distribution

The RTD of a passive tracer in both the helically coiled and chaotic twisted pipe flows was obtained experimentally using a conductimetric method with two measurement points [7,12,13]. The concentration of an injected tracer was sampled, as a function of time, at both the inlet and the outlet of the geometry under study. To ensure uniform tracer concentration at the entrance of the twisted pipe, the tracer injection was followed by a seven-element Sulzer SMX static mixer, which extends the time distribution of the tracer at the inlet and thus allows a correct sampling of the signal coming from the injection by means of a syringe. Depending on the Reynolds numbers range under study (see Table 1), pure water or saccharose solutions were used as working fluids, the tracer being a solution of sodium hydroxide (NaOH). When water is the working liquid, between 0.5 and 2 cm^3 of 0.25 mol l^{-1} NaOH solution were injected, whereas about 2 cm^3 of 1 mol l^{-1} NaOH solution were injected when saccharose solutions were involved. This passive tracer was detected using two specially designed conductimetric cells, made up of two semicylindrical nickel plates insulated from each other and having the same diameter as the twisted pipe systems. These self-made cells ensure sampling of the whole volume of the injected tracer. Each sensor is connected to a variable-frequency conductimeter (TACUSSEL CD 810). The frequency of the applied alternating current between the two electrodes of the conductimetric cells was fixed at 1 kHz in order to ensure a linear relationship between the conductivity and the concentration of the tracer in the corresponding range ($0 \leq C \leq 1$ mol l^{-1}). The concentration curves at the inlet, $C_1(t)$, and at the outlet, $C_2(t)$, of the geometry under study are sampled at a frequency varying between 7 and 60 Hz (depending on the flow rate) by means of a data-acquisition device (AOIP SA 32) connected to a personal computer for data processing (see Fig. 1).

The use of a two-measurement-point method instead of the more common step or pulse injection modes [14], while making the determination of the parameters of any flow model more intricate [15,16], avoids the experimental difficulties involved in obtaining a perfect pulse or step injection. It also allows easy verification of the tracer balance by integration and comparison of the two experimental signals, $C_1(t)$ and $C_2(t)$. In all experimental data discussed here, the tracer balance is correct to less than 10%.

As mentioned above, after the injection of the tracer (NaOH), the liquid was not recycled in the flow loop, but was instead stored in a secondary reservoir (Fig. 1), so as to avoid modifying the conductivity of the basic feed. The small quantities of injected tracer ensure that the physical properties of the working solutions remain unchanged throughout the experiments.

3. Modeling of RTD and experimental results

3.1. Choice of the model and modelling

In a previous work, Castelain et al. [7] used the axial dispersed plug flow model to characterise RTD curves of a liquid flowing through the same devices used here (see Fig. 2) for high Reynolds numbers ($800 \leq Re \leq 13{,}000$; see Table 1). For this Reynolds numbers range, the flow in the chaotic twisted pipe arrangement can be considered as fully chaotic in the whole section of the apparatus [7,2]. In this case, the dispersed plug flow model has been found suitable for correct prediction of the RTD of the liquid, both in the chaotic and in the helically coiled systems [7], confirming previous experimental work dedicated to this last configuration [17,18,4]. Here, the experimental RTD curves obtained in the chaotic device and in the helically coiled tube were also analysed using the plug flow with axial dispersion model. The simplicity of this model allows it to be used for chemical engineering design in various geometries, such as axial flow in straight pipes [19]; Couette flow [20], Taylor-Couette flows [21] or annular swirling decaying flow induced by means of a tangential inlet [12,13]. In the dispersed plug flow model, a dispersion in the main flow direction, due to local velocity fluctuations, is superimposed on the ideal plug flow. These velocity fluctuations are introduced through an axial, or longitudinal, dispersion coefficient, D_{ax}, in a relationship analogous to Fick's diffusion law. For low flow rates, D_{ax} accounts for the combined dispersive effects coming from molecular dispersion and convective contribution [19]. For flows of forced convection type, like those investigated here, the effects of molecular diffusion can be assumed negligible. The concentration, C, of a passive tracer uniformly injected within the inlet cross-section of the device is given as a function of time, t, and streamwise coordinate, z, by:

$$\frac{\partial C}{\partial t} = D_{ax}\frac{\partial^2 C}{\partial z^2} - \bar{W}\frac{\partial C}{\partial z} \tag{1}$$

where $\bar{W}$ is the mean axial flow rate. In relation (1), the concentration of the sampling species, C, is assumed constant within each cross-section of the flow field (no radial dispersion) and the axial dispersion coefficient, D_{ax}, is considered independent of both the tracer concentration and the longitudinal coordinate, z. Obviously, the last assumption is not completely fulfilled in our chaotic configuration, for which Castelain et al. [7] have shown that D_{ax} depends on the number

of bends constituting the device, and thus evolves along the flow path. Indeed, the flow characteristics are not fully established as soon as the fluid enters the system. For instance, in the helically coiled tube, the Dean roll-cells [9,10] are not well developed in the first bends of the apparatus. Furthermore, in the first few elbows of the chaotic twisted pipe flow, chaotic flow regions can coexist with regular zones [2,22], which obviously implies an evolution of the axial dispersion coefficient along the flow path. Thus D_{ax} must be considered as a mean value, which is still appropriate for global characterisation of the dispersive effects of a given flow.

The plug flow with axial dispersion model is characterised by two parameters, the mean residence time of the fluid in the system, $\overline{t_s}$, and the Péclet number based on the total length, L, between the two sensors, $Pe_L = \bar{W}L/D_{ax}$; these are determined using curve-fitting in the time domain [23,15]. This appears to be the most accurate way to identify the different parameters involved in a given flow model from measurement of tracer input and response signals [16]. This method is based on comparison of the experimental concentration outlet curve and that calculated, in the time domain, using the inlet curve concentration signal and the transfer function of the flow model. The inlet, $C_1(t)$, and outlet, $C_2(t)$, concentration curves are first normalised to ensure exact satisfaction of the tracer balance, and then expressed in terms of Fourier series [23,15,13,24]. The resolution of Eq. (1), using the Laplace transform, allows the determination of the transfer function $F_1(s) = C_{2calc}(s)/C_1'(s)$ between Laplace transforms of the normalised calculated outlet signal and the experimental inlet curve.

For the dispersed plug flow model, when axial dispersion extends before the inlet detector and after the outlet detector (open–open plug flow model with axial dispersion), $F_1(s)$ is given by [25]:

$$F_1(s) = \exp\left\{\frac{Pe_L}{2}\left[1 - \left(1 + \frac{4s}{Pe_L}\overline{t_s}\right)^{1/2}\right]\right\} \tag{2}$$

The predicted temporal normalised response concentration curve, $C'_{2calc}(t)$, can thus be calculated using the definition of the transfer function in the Fourier domain and the normalised inlet signal, $C_1'(t)$:

$$F_1(i\omega) = \frac{\int_0^{2T} C'_{2calc}(t)\exp(-i\omega t)\,dt}{\int_0^{2T} C_1'(t)\exp(-i\omega t)\,dt} \tag{3}$$

ω being the pulsation of the Fourier series and $2T$ the time in which the tail of the response signal, $C_2'(t)$, vanishes.The experimental, $C_2'(t)$, and predicted, $C'_{2calc}(t)$, response curves are compared by evaluating the root mean square error, RMS, between these two signals [15]:

$$\mathrm{RMS} = \left[\frac{\int_0^{2T}\left\{C_2'(t) - C_{2calc}(t)\right\}^2 dt}{\int_0^{2T}\left\{C_2'(t)\right\}^2 dt}\right] \tag{4}$$

RMS, which is a function of the two parameters, $\overline{t_s}$ and Pe_L, of the plug flow with axial dispersion model, is minimised using the Rosenbroock optimisation algorithm [26]. As recognised by Rangaiah and Krishnaswamy [27], Pe_L and $\overline{t_s}$ are determined jointly and are assumed to be correctly optimised when RMS remains less than 10%.

As previously observed by Castelain et al. [7], for Reynolds numbers less than about 2500, the agreement between the plug flow with axial dispersion model and the experimental residence time distributions in the chaotic curved-pipe arrangement is not as satisfactory as it is for Reynolds numbers larger than 2500: the root mean square error between the experimental and modelled outlet signals, RMS in Eq. (4), is often larger than 10%. This is mainly due to the tails on the experimental RTD, which cannot be correctly predicted using the dispersed plug flow model. These tails were also observed by Jones and Young [28] in a theoretical investigation of dispersion of a passive scalar in steady viscous flow through a twisted pipe subject to chaotic advection. The flow can thus be considered as a mixed regime in which islands of integrable trajectories coexist within irregular regions [2,28]. The trajectories of fluid particles do not instantaneously become fully chaotic as the fluid enters the twisted pipe system. At the inlet of the apparatus, small regions where the flow becomes less and less regular appear; these spread along the flow path and finally cover the whole cross-section. The transition between these two asymptotic flow regimes is characterised by the coexistence of chaotic zones with regular parts, and this competition induces tails on the RTD curves. Thus, for Reynolds numbers less than about 2500, the experimental RTD was modelled using a plug flow with axial dispersion part that exchanges mass with a stagnant region. This model was first used by Coats and Smith [29] to study the flow in porous media including dead-end pore volumes, which cannot be predicted by the single plug flow with longitudinal dispersion model since it cannot reproduce the asymmetry of the response signal to a tracer injection. The dispersed plug flow model exchanging mass with a stagnant volume has also been successfully used by Piva et al. [30] to investigate a Taylor–Couette–Poiseuille flow in which the injected passive tracer remains partly trapped within the Taylor counter-rotating vortices, while the remaining tracer flows along the separatrices of the vortices without

penetrating them. In such a flow, Piva et al. [30] have shown that the stagnant zone can represent 30% of the total volume of the apparatus. More recently, Legentilhomme and Legrand [12] also employed this model in swirling annular or tubular decaying flow in which a large recirculation bubble, quite stagnant in part of the cell, appears. The dispersed plug flow model exchanging mass with a stagnant volume is expressed by the following two differential equations [29]:

$$D_{ax}\frac{\partial^2 C}{\partial z^2} - \bar{W}\frac{\partial C}{\partial z} = f\frac{\partial C}{\partial t} + (1-f)\frac{\partial C^*}{\partial t} \tag{5}$$

$$(1-f)\frac{\partial C^*}{\partial t} = K(C - C^*) \tag{6}$$

where C^* is the tracer concentration in the stagnant zone, f the fraction of the volume subjected to plug flow with axial dispersion, and K the mass transfer coefficient between the flowing volume and the stagnant region.

Applying the Laplace transform to Eqs. (5) and (6), the transfer function of this model, $F_2(s)$, can be established as:

$$F_2(s)\frac{2\beta^{1/2}\exp\left\{\frac{1}{2}\left[Pe_L - \beta^{1/2}\right]\right\}}{\left(Pe_L + \beta^{1/2}\right) - \left(Pe_L - \beta^{1/2}\right)\exp\left\{-\beta^{1/2}\right\}} \tag{7}$$

with $\beta = Pe_L^4 + 4s\gamma Pe_L\overline{t_s}$; $\gamma = f + \frac{G(1-f)}{\overline{t_s}(1-f)s+G}$; and $G = \frac{KL}{\bar{W}}$.

This model involves four parameters, $\overline{t_s}, G, f$ and Pe_L, the optimisation of which is very difficult without a good initial estimate. As in the dispersed plug flow model, $\overline{t_s}$ is initialised using the first moment of the residence time distribution. G and f are first estimated assuming that plug flow occurs in the non-stagnant zone. With this assumption, $F_2(s)$ reduces to:

$$F_3(s) = \exp\left\{-s\left[f + \frac{G-f}{\overline{t_s}s(1-f)+G}\right]\overline{t_s}\right\} \tag{8}$$

The values of G, f and $\overline{t_s}$ obtained using $F_3(s)$ are then fixed in the transfer function (7) in order to obtain a first value of Pe_L. Finally, the four parameters of the plug flow with axial dispersion model exchanging mass with a stagnant zone are globally optimised from the previous estimation. This procedure has been shown to be robust by Legentilhomme et al. [13].

3.2. Experimental results

The dispersed plug flow model is not suitable for simulating the dispersion process, especially for small Reynolds numbers for which RMS is often larger than 10%. The second model, associating a dispersed plug flow exchanging mass with a dead zone, appears better: the RMS between the experimental and calculated outlet signals remains less than 10% over the whole Reynolds numbers range.

An example of curve-fitting is given in Fig. 3 for a 33-bend configuration system ($Re = 448$). The RMS is equal to 21.8% if the plug flow with axial dispersion model is used (Fig. 3(a)), whereas it is reduced to 5%

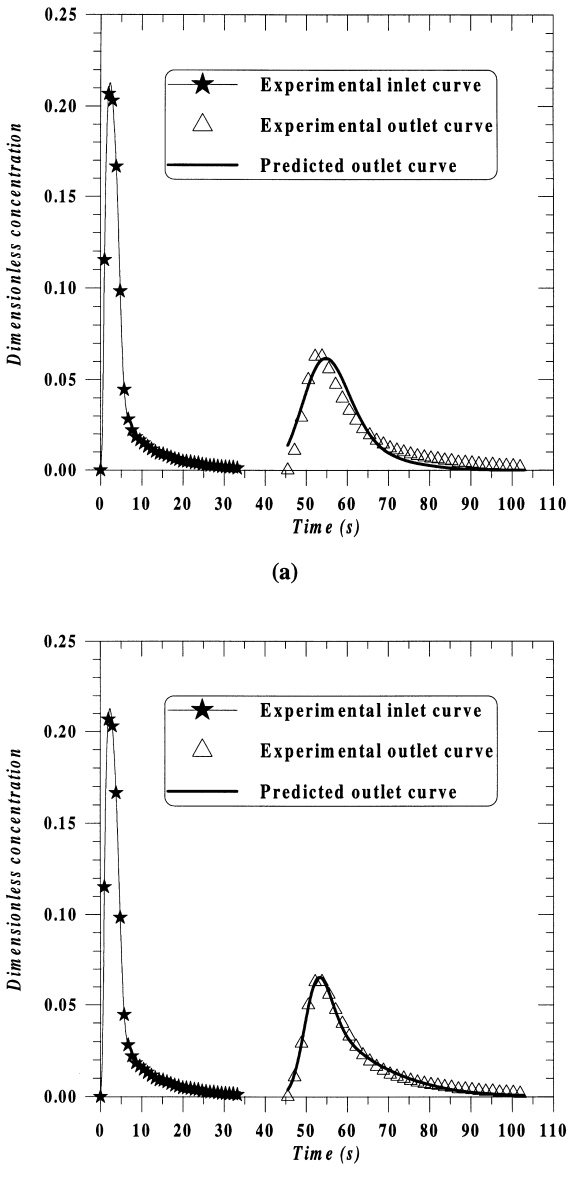

Fig. 3. An example of curve-fitting in time domain using the two models (33-bend chaotic system, $Re = 448$): (a) plug flow model with axial dispersion; (b) dispersed plug flow model exchanging mass with a stagnant zone.

with the dispersed plug flow model exchanging mass with a stagnant zone (Fig. 3(b)).

Fig. 4 depicts the variation of the Péclet number based on the tube diameter as a function of the Reynolds number for several chaotic configurations. The Péclet number increases with an increase in Reynolds number, whatever the number of bends constituting the system. When the Reynolds number increases, the decrease in axial dispersion is due to the secondary flow. In curved pipes, the secondary flow due to the appearance of Dean vortices [9,10] is expected to increase transverse mixing and to flatten the concentration distribution in the cross-section of the device. Nunge et al. [31] have observed, for laminar flow in a helically coiled system, that when the Reynolds number increases, the effective axial dispersion decreases due to the action of the secondary flow. In addition, in chaotic twisted pipe flow, the reduction of the RTD is more pronounced because of another mechanism: the generation of chaotic trajectories in the flow. This phenomenon also accounts for an increase in transverse dispersion [32] because, before leaving the system, fluid elements can visit many transverse positions and thus move at different velocities.

Fig. 5 shows the variation of the volume fraction subjected to plug flow with axial dispersion as a function of the Reynolds number for different configurations tested. Globally, the flowing fraction, f, increases with Reynolds number, whatever the number of bends, to reach a maximum value varying from 0.9 to 1. For Reynolds numbers between 50 and 200, the flowing fraction increases with the number of bends involved in the chaotic twisted pipe flow. The nature of the flow regime depends on the angular extension of the bends, the angle between the plane of curvature of two successive bends and the Reynolds number [28]. For instance, when the number of bends or the Reynolds number is small, some streamlines are confined in streamtubes where the flow remains regular, whereas other trajectories become chaotic, inducing what is usually called a 'mixed regime'. If all trajectories become non-integrable, the flow is fully chaotic. This suggests that the flow regime is of transitional type and can thus be classified between purely regular and chaotic flows. Such an intermediate regime could contain limited regions where trajectories remain regular and other zones where trajectories become more and more complex. In this case, the stagnant zones of the model described by Eqs. (5) and (6) should be associated with the fluid particles located close to the tube wall, where the axial velocity is very low. They remain trapped near the tube wall and thus should need a longer time to reach the exit of the geometry. A radial transport mechanism inherent to molecular diffusion allows these particles to move towards the central core of the tube, which can be primarily characterised by essentially plug flow. When the tube length is increased, the chaotic zones begin to extend towards the regions close to the wall, allowing more trapped particles to escape from the stagnant zone and move towards the tube central core. In fact, the radial transport mechanism is much more efficient in the chaotic zones than in the regular ones, where only molecular

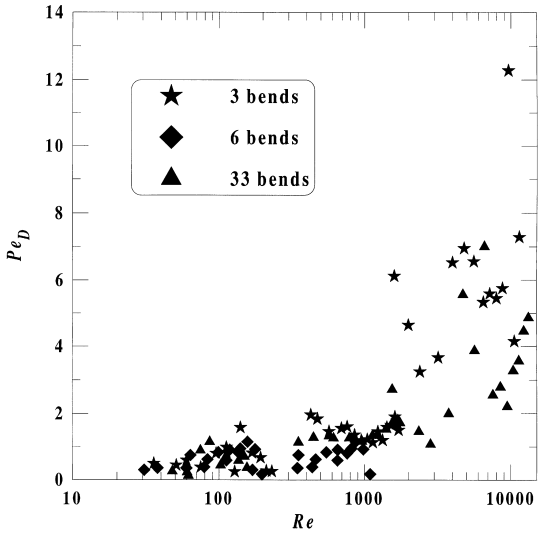

Fig. 4. Péclet number based on the diameter versus Reynolds number for different configurations of the chaotic system. Dispersed plug flow model exchanging mass with a stagnant zone.

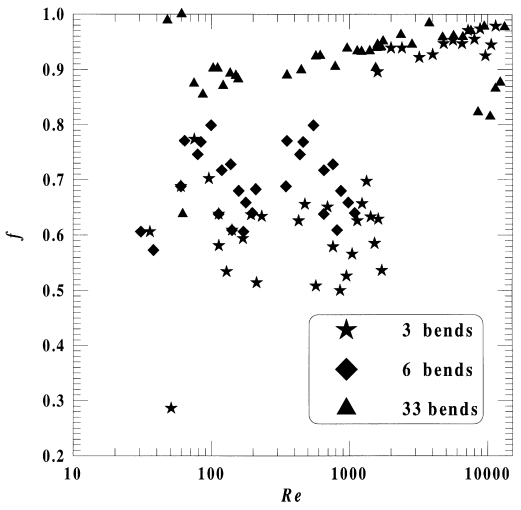

Fig. 5. Evolution of the flowing fraction versus Reynolds number for different configurations of the chaotic system. Dispersed plug flow model exchanging mass with a stagnant zone.

diffusion takes place. This mechanism of development for chaotic trajectories may explain why the stagnant zone is reduced when the number of bends is increased. It should be noted that this mechanism has already been observed in previous studies [28,32].

The dispersion coefficient is not a sufficient criterion for characterising and comparing mixing device performance. In fact, this parameter characterises mixing performance globally without taking into account any eventual increase in pressure drop, which appears to be an important parameter from an energetic point of view. In order to further characterise the efficiency of a given device, we suggest the use of another criterion that takes into account the pressure drop via a friction factor:

$$C_r = \frac{\nu}{D_{ax} C_f} \tag{9}$$

For the same pressure drop, the criterion increases when the axial dispersion decreases; for the same axial dispersion, the criterion increases when the pressure drop decreases. Fig. 6 presents the evolution of this criterion for two chaotic systems consisting of 3- and 33-bends for different Reynolds numbers. In the 3- or 33-bend chaotic configuration, the criterion decreases with the Reynolds number. The pressure drop induced by the increase of the flow rate is more important than the decrease in axial dispersion. The criterion was calculated for a straight tube and a helical device by using data from Sakra et al. [33] and Mishra and Gupta [34], and for an annular swirling decaying flow induced by means of a tangential inlet [12,35]. The axial dispersion coefficient was obtained by using the axial dispersion model. The criterion is more important in the chaotic configuration.

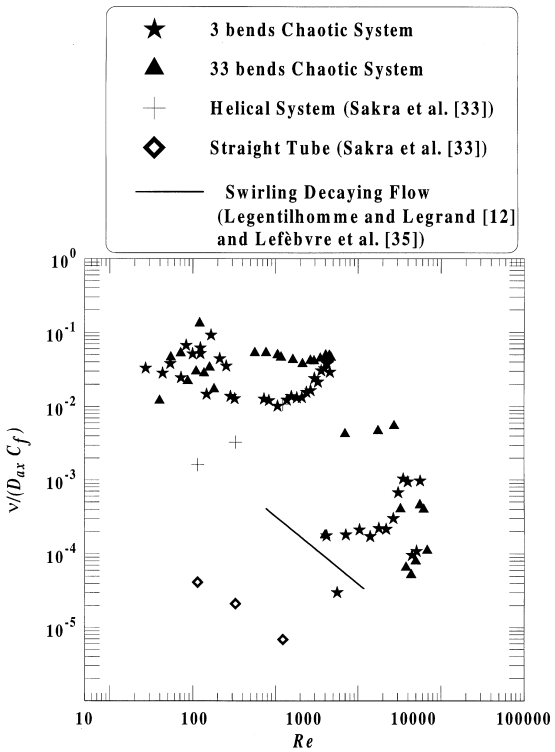

Fig. 6. Evolution of the mixing criterion of the chaotic system versus Reynolds number. Comparison with other works.

4. Numerical simulation of the RTD

4.1. Evaluation of the RTD

The present numerical simulation of the chaotic twisted pipe flow is based on a simplified model developed by Jones et al. [2] that uses the approximate velocity fields for flow in a curved pipe of circular cross-section previously developed by Dean [9,10]. The flow field is assumed to be steady, incompressible and fully developed in the whole geometry. The equations of motion are written in the two toroidal local coordinate systems (x, y, θ) and (r, φ, θ) shown in Fig. 7. The relation between the two systems is:

$$x = r\sin(\varphi)$$

$$y = r\cos(\varphi) \tag{10}$$

Non-dimensionalising all lengths by r, the axial velocity, w, by the average axial velocity, $\bar{W}$, and the stream function, ψ, by the kinematic viscosity, ν, leads to the following dimensionless equations for w and the secondary flow stream function, ψ [36]:

$$\nabla^2 w = \frac{1}{r}\left(\frac{\partial\psi}{\partial r}\frac{\partial w}{\partial\varphi} - \frac{\partial\psi}{\partial\varphi}\frac{\partial w}{\partial r}\right) - A$$

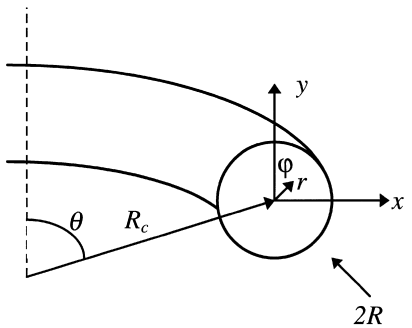

Fig. 7. Local coordinate system used for the numerical simulation.

$$\nabla^4\psi = \frac{1}{r}\left(\frac{\partial\psi}{\partial r}\frac{\partial}{\partial\varphi} - \frac{\partial\psi}{\partial\varphi}\frac{\partial}{\partial r}\right)\nabla^2\psi + 2Dn^2 w\left(\frac{\sin\varphi}{r}\frac{\partial w}{\partial\varphi} - \cos\varphi\frac{\partial w}{\partial r}\right) \quad (11)$$

Here A is a dimensionless number expressing the overall pressure gradient driving the flow:

$$A = -\frac{R^2}{\mu\bar{W}}\frac{\partial P}{R_c\partial\theta} \quad (12)$$

and Dn is the Dean number given by

$$Dn = \frac{\bar{W}R}{\nu}\sqrt{\frac{D}{R_c}} \quad (13)$$

For small values of the Dean number up to values of the order of 30, Dean [9,10] solved Eq. (11) using a perturbation method. The perturbation solution is obtained by expanding w and y in a power series of $2Dn^2$. In the local coordinate system (x, y, θ), the secondary velocities u and v can be written as:

$$u = \frac{\partial\psi}{\partial y} \qquad v = -\frac{\partial\psi}{\partial x} \quad (14)$$

Limiting the power series to the first order of $2Dn^2$ and considering the pressure gradient to remain the same as that in a straight pipe in laminar flow regime leads to:

$$\frac{\partial P}{R_c\partial\theta} = \frac{\partial P}{\partial z} = \frac{-8\mu\bar{W}}{R^2} \quad (15)$$

By solving Eq. (11), Dean [9,10] showed that the secondary velocities are given by the following two equations:

$$u = \frac{A^2Dn^2}{4468}\left(1-x^2-y^2\right)\left(4-5x^2-23y^2+8x^2y^2+x^4+7y^4\right)$$

$$v = \frac{A^2Dn^2}{1152}\left(1-x^2-y^2\right)xy\left(3-x^2-y^2\right) \quad (16)$$

Thus, in the local coordinate system (x, y, θ), the axial velocity component is given by Refs. [9,10]:

$$w = \frac{R_c\partial\theta}{\partial t} = \frac{2Dn^2}{Re}\left(1-x^2-y^2\right) \quad (17)$$

Since the flow is steady, the system $(u, v, w) = [\frac{dx}{dt}, \frac{dy}{dt}, \frac{dz}{dt}]$ is autonomous and the independent variable can be changed from time t to angular position θ by dividing Eq. (16) by Eq. (17), [2]. This simplification reduces the dynamical system to two equations:

$$\frac{dx}{d\theta} = \frac{Re}{144}\left(4-5x^2-23y^2+8x^2y^2+x^4+7y^4\right)$$

$$\frac{dy}{d\theta} = \frac{Re}{24}xy\left(3-x^2-y^2\right) \quad (18)$$

The system of two differential Eq. (18) defines the mapping of fluid particles in the cross-sectional plane at a given θ value. In a helically coiled configuration formed by the succession of n 90° bends, particle trajectories are obtained by integration of system (18) following θ between 0 and the final angular coordinate. In that procedure, torsion effects are neglected. For the chaotic case, particle trajectories are obtained by integration of system (18) between the beginning and the end of each bend. At the end of each bend, the coordinate system is changed. If the angle between the curvature plane of two successive bends is α, the new coordinate system is obtained by a rotation $-\alpha$ of the previous coordinate system corresponding to the preceding elbow. We assume that the flow becomes fully developed as soon as it enters the bend, and that, as the flow leaves one bend to enter the next, the readjustment from one secondary flow pattern to another is immediate. The system (18) is numerically integrated using a fourth-order Runge–Kutta method. All the calculations were performed in double precision.

The RTD of a passive tracer is obtained numerically by injecting a series of Dirac functions of passive tracer particles uniformly distributed within the cross-section at the entrance of the system. The amplitude of each successive Dirac function is chosen so as to reconstruct the shape of the experimental injection at the entrance. However, it should be noted that the results are independent of the shape of the injection curve. This way of reconstructing the injection curve is chosen to avoid modifying the transfer function in the numerical study. Thus, the inlet numerical curve obeys a parabolic equation. The total number of particles is 250,000, whatever the Reynolds number. The number of particles in each elementary Dirac injection corresponds to the injected tracer concentration during each pulse duration. Thanks to the simple flow model presented above, we can calculate the trajectories of the fluid particles, in order to obtain their residence time and the cross-sectional position of each injected particle. The entrance curve shape does not influence the RTD, which depends only on the flow field. Thus we can establish an outlet histogram built using the number of particles reaching the exit of the system in a given residence time interval.

4.2. Results

Computations were performed for Reynolds num-

bers between 10 and 100, in helically coiled and chaotic systems made of 3, 6, 9 and 33 bends, and the results were analysed with the different models described above. As was true for the experimental data, the RMS between the calculated and the numerically simulated outlet curves using the plug flow with axial dispersion model is rather high, especially for smaller values of the Reynolds number and for systems having a large number of bends. The main difficulty arises from the tail of the response curve coming from slower particles that take more time to leave the system. For small Reynolds numbers, fluid particles close to the walls have difficulty in reaching the exit of the system. The dispersed plug flow model does not correctly describe the spread of the RTD. In order to overcome this problem, the dispersed plug flow model exchanging mass with a stagnant zone was used for all the configurations investigated numerically. Fig. 8 compares the Péclet number in helically coiled and chaotic systems for the 3- and 33-bend configurations. Globally, the Péclet number is larger in the chaotic system (a large Péclet number indicates a small axial dispersion). A previous study has already pointed out that the axial dispersion was lower in the chaotic system than in the helically coiled one for large Reynolds numbers ($Re > 800$, [7]). The same tendency is observed here for smaller Reynolds numbers. The evolution of the flowing fraction is presented in Figs. 9 and 10, respectively, for the helically coiled and chaotic twisted pipe systems for different Reynolds numbers. Flowing fraction values are distributed around a mean value of 0.65 for the helically coiled system. By the hy-

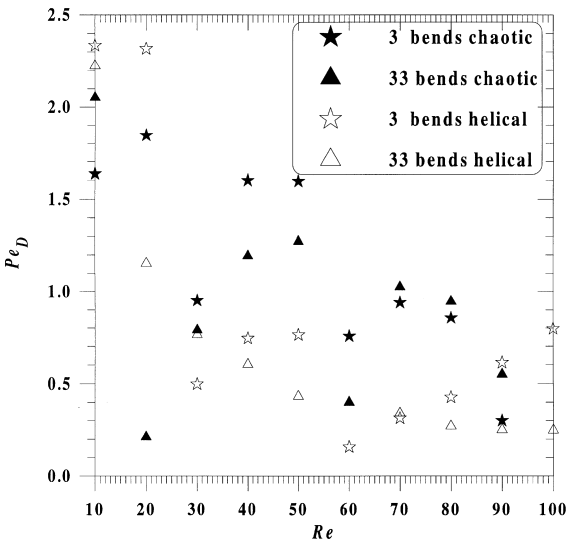

Fig. 8. Evolution of the Péclet number based on the diameter versus Reynolds number for the helically coiled and chaotic systems. Numerical results.

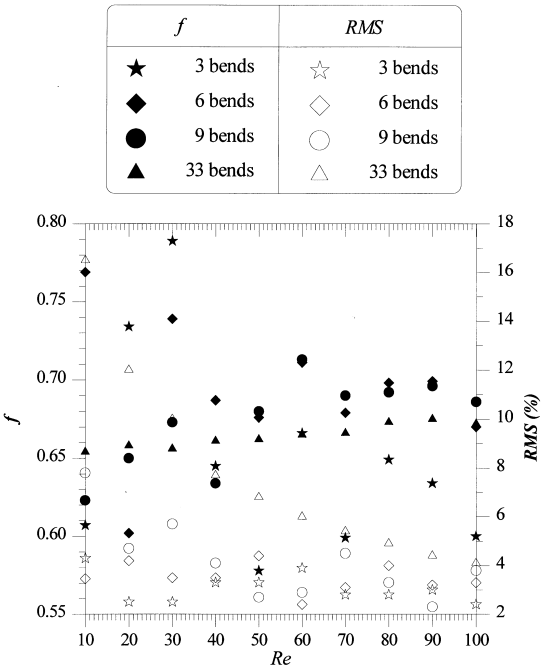

Fig. 9. Evolution of the flowing fraction versus Reynolds number for different configurations of the helically coiled system. Numerical results.

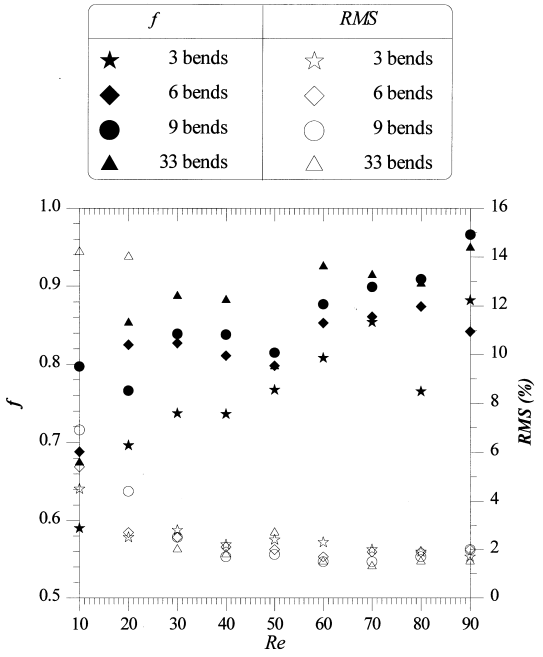

Fig. 10. Evolution of the flowing fraction versus Reynolds number for different configurations of the chaotic system. Numerical results.

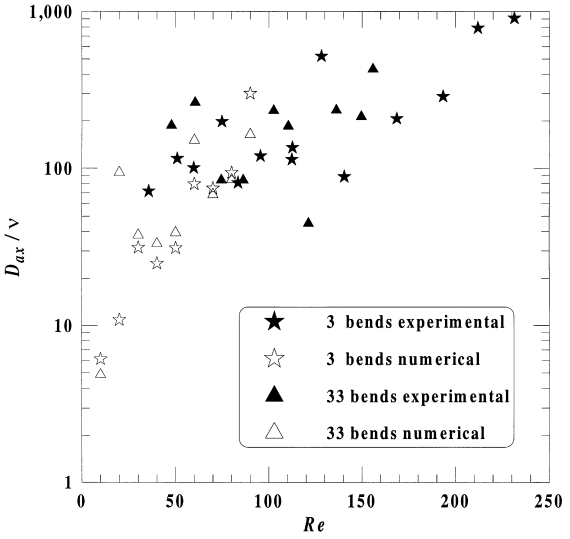

Fig. 11. Comparison of the numerical and experimental axial dispersion, D_{ax}/ν, vs. Re.

pothesis of the simulation, Dean vortices are established as soon as the fluid enters each bend, and a constant value of the flowing fraction is stabilized after six bends. Furthermore, the flowing fraction stability with Reynolds number can also be attributed to the fact that the Dean vortices have the same size, whatever the Reynolds number. Unlike the helically coiled geometry, the flowing fraction in the chaotic system is not constant (Fig. 10): variations are observed as a function both of the number of bends and of Reynolds number. Globally, the flowing fraction increases with increasing Reynolds number, whatever the number of bends involved in the chaotic mixer. This evolution is mainly due to the initiation of a mixed regime, as discussed in Section 3 above.

Fig. 11 compares the experimental and numerical axial dispersion coefficients in chaotic systems in terms of the ratio D_{ax}/ν versus Reynolds number. The numerical results are in good agreement with experimental data in the common range of Reynolds numbers ($20 \leq Re \leq 100$). In the two cases, RTD was modelled using the dispersed plug flow model exchanging mass with a stagnant zone.

5. Conclusions and discussion

The experimental evaluation of RTD in a spatially chaotic system associated with the use of a dispersed plug flow exchanging mass with a stagnant zone has allowed the determination of a global axial dispersion coefficient. For small Reynolds numbers, the tails appearing on the experimental RTD are correctly predicted in this model.

When the Reynolds number is increased, the axial dispersion coefficient decreases, whatever the number of bends in the system. In chaotic twisted pipe flow, the reduction in the RTD is due to the appearance of the secondary flow and to the initiation of chaotic trajectories in the flow. This phenomenon contributes to an increase in transverse dispersion.

The flowing fraction increases with Reynolds number, whatever the number of bends in the chaotic mixer, and reaches a maximum value varying from 0.9 to 1. For Reynolds numbers between 50 and 200, the flowing fraction increases with increasing the number of bends. When the number of bends or the Reynolds number is small, some streamlines are confined in streamtubes where the flow remains regular, whereas other trajectories become chaotic, creating a mixed flow regime.

A dispersion model was developed that takes into account this particular regime. The presence of chaotic and regular zones suggests modelling the flow with two parallel zones:

- a first zone modelled by a perfect mixed tank (this zone can be assimilated to the chaotic regions),
- a second part modelled by a plug flow with axial dispersion (this zone can be assimilated to the regular part of the flow).

The size of these zones varies along the mixer. At the inlet, the regular zone is predominant, but after a few bends, the fully developed chaotic zone begins to cover the main part of the flow cross-section.

To be valid, the model must take into account the long tailed curves arising from the competition between the two parallel flows. Fluid particles located in the chaotic regions should take longer to flow through the geometry than particles flowing in the regular zones. However, this model was unsatisfactory in that it led to RMS values greater than 20% between the experimental and calculated response concentration signals. The plug flow model with axial dispersion exchanging mass with a dead zone was found to be the more appropriate model. A mixing efficiency criterion was suggested to take into account both mixing quality and the associated pressure drop. Residence time distributions were also obtained numerically using a flow model based on Dean's perturbation solutions of the Navier–Stokes equations in helically coiled and chaotic systems. The average Péclet number obtained in the chaotic configuration is higher than that in the helically coiled configuration. The evolution of the flowing fraction has revealed different behaviours in the two kinds of flow. Numerical results are in good agreement with corresponding experiments.

References

[1] H. Aref, Stirring by chaotic advection, J. Fluid Mech 143 (1994) 1–21.

[2] S.W. Jones, O.M. Thomas, H. Aref, Chaotic advection by laminar flow in twisted pipe, J. Fluid Mech 209 (1989) 335–357.

[3] Y. Le Guer, H. Peerhossaini, Order breaking in Dean-flow, Phys. Fluids A3 (1991) 1029–1032.

[4] A.K. Saxena, K.P.D. Nigam, Axial dispersion in laminar flow of polymer solutions through coiled tubes, J. Appl. Polymer Sci 26 (1981) 3475–3486.

[5] J.M. Ottino, The Kinematic of Mixing, Cambridge University Press, Cambridge, 1989.

[6] E. Villermaux, J.P. Hulin, Chaos lagrangien et mélange de fluides visqueux, Eur. J. Phys 11 (1990) 179–183.

[7] C. Castelain, A. Mokrani, P. Legentilhomme, H. Peerhossaini, Residence time distribution in twisted pipe flows: helically coiled and chaotic systems, Exp. Fluids 22 (1997) 359–368.

[8] H. Peerhossaini, C. Castelain, Y. Le Guer, Heat exchanger design based on chaotic advection, Exp. Therm. Fluid Sci 7 (1993) 333–344.

[9] W.R. Dean, Note on the motion of fluid in a curved pipe, Phil. Mag 4 (1927) 208–227.

[10] W.R. Dean, The streamline motion of fluid in curved pipe, Phil. Mag 5 (1928) 673–695.

[11] A. Mokrani, C. Castelain, H. Peerhossaini, The effects of chaotic advection on heat transfer, Int. J. Heat Mass Transfer 40 (1997) 3089–3104.

[12] P. Legentilhomme, J. Legrand, Distribution des temps de séjour en écoulement tourbillonnaire annulaire induit par une entrée tangentielle du liquide, Can. J. Chem. Eng 73 (1995) 435–443.

[13] P. Legentilhomme, L. Brujes, J. Legrand, Distribution des temps de séjour du liquide en écoulement annulaire tourbillonnaire non-entretenu liquide–solide: influence de la présence de solide, Chem. Eng. J 67 (2) (1997) 83–96.

[14] J. Villermaux, Génie de la réaction chimique. Conception et fonctionnement des réacteurs, Eds. Technique et Documentation, Lavoisier, Paris, 1984.

[15] N. Wakao, S. Kaguei, Heat and Mass Transfer in Packed Beds, Gordon and Breach, London, 1982.

[16] M.A. Fahim, L.T. Wakao, Parameter estimation from tracer response measurements, Chem. Eng. J 25 (1982) 1–8.

[17] R.N. Trivedi, K. Vasudeva, RTD for diffusion-free laminar flow in helical coils, Chem. Eng. Sci 29 (1974) 2291–2295.

[18] R.N. Trivedi, K. Vasudeva, Axial dispersion in laminar flow in helical coils, Chem. Eng. Sci 30 (1975) 317–325.

[19] G. Taylor, Dispersion of soluble matter flowing slowly through a tube, Proc. Roy. Soc. Ser A219 (1953) 186–203.

[20] P.I. Pudjiono, N.S. Tavare, J. Garside, K.P.D. Nigam, Residence time distribution from a continuous Couette flow device, Chem. Eng. J 48 (1992) 101–110.

[21] J. Legrand, F. Coeuret, Circumferential mixing in one-phase and two-phase Taylor vortex flow, Chem. Eng. Sci 41 (1986) 47–53.

[22] C. Castelain, Etude expérimentale de la dynamique des fluides et des transferts thermiques dans un écoulement de Dean alterné en régime d'advection chaotique, Ph.D. dissertation, ISITEM, University of Nantes, 1995.

[23] W.C. Clements, A note on determination of the parameters of the longitudinal dispersion model from experimental data, Chem. Eng. Sci 24 (1969) 957–963.

[24] P. Legentilhomme, J. Legrand, J. Comiti, Axial dispersion in electrolyte flowing through anisotropic packed beds, J. Appl. Electrochem 19 (1989) 263–270.

[25] C.Y. Wen, L.T. Fan, Models for Flow Systems and Chemical Reactors, Marcel Dekker, New York, 1975.

[26] G.S.G. Beveridge, R.S. Schechter, Optimization: Theory and Practice, McGraw-Hill, New York, 1970.

[27] G.P. Rangaiah, P.R. Krihnaswamy, Application of time domain curve-fitting to parameter estimation in RTD models, J. Chem. Eng. Jap 23 (1990) 124–130.

[28] S.W. Jones, W.R. Young, Shear dispersion and anomalous diffusion by chaotic advection, J. Fluid Mech 280 (1994) 149–172.

[29] K.H. Coats, B.D. Smith, Dead-end pore volume and dispersion in porous media, Soc. Petroleum Eng. J., Trans. AIME 231 (1964) 73–84.

[30] M. Piva, A. Calvo, A. Barrantes, S. Gabanelli, M. Rosen, I. Ippolito, J.E. Wesfreid, Tracer dispersion in the Taylor-Couette instability with axial flow, in: E. Trapegui, W. Zeller (Eds.), Instabilities and Non-Equilibrium Structures IV, Kluwer Academic Publishers, Dordrecht, 1993.

[31] R.J. Nunge, T.S. Lin, W.N. Gill, Laminar dispersion in curved tubes and channels, J. Fluid Mech 51 (1972) 368–383.

[32] C. Castelain, A. Mokrani, Y. Le Guer, H. Peerhossaini, Experimental study of chaotic advection regime in a twisted duct flow, Eur. J. Mech. (1999), accepted.

[33] T. Sakra, F. Lesek, H. Cermankova, Axial dispersion in a reactor with a helical flow, Collection Czechoslov. Chem. Commun. 36 (1971).

[34] P. Mishra, S.N. Gupta, Momentum heat transfer in curved pipes. Part I: Newtonian fluids, Ind. Eng. Chem. Process Des. Dev 18 (1978) 130–137.

[35] G. Lefèbvre, S.R. Farias Neto, H. Aouabed, P. Legentilhomme, J. Legrand, Transfert de matière et chute de pression lors d'un écoulement tourbillonnaire annulaire non entretenu induit par une entrée tangentielle, Can. J. Chem. Eng 79 (1998) 1039–1050.

[36] S.A. Berger, L. Talbot, L.S. Yao, Flow in curved pipes, Ann. Rev. Fluid Mech. 1 (1983) 461–512.